Journal of Manufacturing Processes 84 (2022) 43–54

Contents lists available at ScienceDirect

Journal of Manufacturing Processes

journal homepage: www.elsevier.com/locate/manpro

On modelling coolant penetration into the microchannels at the tool-workpiece interface

Wenming Wei [a,b], Jose A. Robles-Linares [a,*], Zhirong Liao [a,*], Zhao Wang [a], Gonzalo Garcia Luna [a], John Billingham [c], Dragos Axinte [a,d]

[a] Machining and Condition Monitoring Group, Faculty of Engineering, University of Nottingham, UK
[b] School of Mechanical Engineering, Xi'an Jiaotong University, Xi'an, ShaanXi 710049, China
[c] School of Mathematical Sciences, University of Nottingham, UK
[d] Faculty of Science and Engineering, University of Nottingham Ningbo China, Ningbo, China

ARTICLE INFO

Keywords:
Metal cutting
Inconel 718
Multiscale model
Coolant penetration
Lubrication

ABSTRACT

A network of microchannels is formed at the interface between the cutting tool and the workpiece during machining due to their rough surface structures. The penetration of coolant into these microchannels has a great effect on the machined surface quality by changing the frictional behaviour and heat transfer characteristics of the interfaces. Most of the present studies focus on the macroscopic coolant delivery process but the mechanism of the microscopic penetration phenomena in the channels at the interface remains unclear. Thus, this study proposes a multi-scale and multi-phase comprehensive theoretical model by combining the machining process, coolant flowing in microchannels and lubrication process, to analyse the coolant transportation in the microchannels and investigate its lubrication effects and the friction mechanisms at the interface between the tool and the workpiece. Then, an orthogonal turning testing of Inconel 718 is designed to verify the proposed model. The cooling and lubrication effect of coolant in the microchannels on the reduction of tool wear, contact length, cutting force and temperature has been demonstrated. And the improvement of chip fragment and microstructure has also been revealed.

1. Introduction

During machining processes, such as milling or grinding, the tool's rake face is in contact with the flowing chip. Due to the cutting action, the chip can exhibit a rough surface that allows for the formation of microcavities or micro-voids in the tool-chip interface, which from here onwards are referred to as 'microchannels'. These microchannels play a major role in the machining process because, when cooling systems are employed, they permit inwards flow towards the cutting edge of the tool, thereby providing a lubrication/cooling capacity locally near the cutting edge and the newly formed chip. Different kinds of coolants are widely used to help with heat dissipation, lubrication, and chip breakage. Among these, the lubrication mechanism in the contact zone has an important effect on coolant efficiency and machined surface quality. The lubrication performance depends on both the coolant flow at the macroscale (i.e., how it interacts with the chip at a large scale) and at the microscale (i.e., how the coolant penetrates the microchannels on the interface between the cutting tool and the chip).

On the macroscale, the coolant properties are determined by the fluid–structure interaction between the coolant, the cutting tool and the chip, which yields an initial pressure and velocity of the coolant at the entrance of the contact zone, thereby changing the interface lubrication status. The normal force exerted on the chip by the coolant pressure changes the chip curvature and reduces the size of the contact zone significantly when a high-pressure water jet is applied [1]. The coolant also alters the breaking mode and morphology of the chips, and introduces tool temperature variation, which in turn alters the velocity field of the coolant flow [2,3]. Additionally, the motion of a rotary tool changes the coolant spatial distribution and the amount of coolant that falls into the wedge cavity formed by the chip and tool's rake face [4]. Moreover, the larger temperatures in the primary and secondary shear zones create a gradient of thermal properties (e.g., thermal conductivity), which also alter the heat dissipation mechanism during the cut [5] and thus result in a complex thermal history upon the machined surface [6] that plays an important role on the surface integrity (e.g., plastic behaviour, grain refinement, micromechanical properties) [7].

* Corresponding authors.
E-mail addresses: Jose.Robles@nottingham.ac.uk (J.A. Robles-Linares), Zhirong.Liao@nottingham.ac.uk (Z. Liao).

https://doi.org/10.1016/j.jmapro.2022.09.044
Received 14 July 2022; Received in revised form 15 September 2022; Accepted 26 September 2022
Available online 5 October 2022

The effect of coolant macro-properties on cutting processes has been extensively studied by both theoretical and experimental methods, including coolant initial parameters, application methods and delivery parameters. The initial velocity and pressure at the exit of the nozzle are determined by the cooling system configuration and can be adjusted by internal pipe layout [8], nozzle shape [9] and atomizer device [10]. The application method depends on the coolant type, and it significantly alters the way the coolant reaches the chip and the tool. The traditional flood method has significant disadvantages, such as high energy consumption, splashing and mist generation [11]. Therefore, scholars have developed various cooling application methods to improve the cutting performance, such as the well-known minimum quantity lubrication (MQL) method [12], high pressure jetting [13] or high-pressure cooling [14] and cryogenic cooling [15]. The latter has been deeply studied both as an external coolant and for internal cooling (i.e., embedded within the tool) [16] and show that cryogenic machining can drastically improve tool life. Furthermore, the delivery parameters (e.g., flow rate, pressure and nozzle position [17,18]) directly affect the coolant's spatial distribution, especially at the entrance of the formed microchannels.

By studying and optimizing the coolant properties at the macroscale, the machining process has been improved greatly by reducing temperature and tool wear, thereby yielding longer tool life and high-quality workpiece. However, these extensive theoretical and experimental studies of coolant properties in the macroscale are far from revealing the mechanism of friction, wear and heat generation in the contact zone. Modifying macro parameters is not always good for the cutting process [19].

On the microscale, the coolant works by penetrating the microchannels with specific initial properties that dramatically change the friction coefficient, heat generation rate and thermal conductivity of the interface. For example, in porous and permeable materials, localised fluid delivery can drastically reduce the friction coefficient in the tool-chip interface [20] and therefore induce a gradient of micro-mechanical properties beneath the machined surface [21]. Nevertheless, the study of fluid delivery upon the cutting zone (at a microscopic level) is a great challenge, since, as defined by Astakhov [22], the high contact pressure between the cutting tool and the workpiece make the fluid through capillaries an intricate problem in which also evaporation is easily enabled. The coolant (in liquid state) usually vaporises (into steam) as a form of heat dissipation mechanism due to the elevated cutting temperatures that are easily achieved during machining. Only a few theoretical investigations related to coolant penetration have been reported. Up to now, only two classical penetration models are available for describing the coolant delivery process on the tool's rake face and both of them are based on the theory of capillarity: (1) the Williams-Tabor penetration model [23,24] and (2) the Godlevski droplet evaporation model [25]. At such a small scale (i.e., at the scale of contact zone during cutting) the coolant behaviour is typically studied with CFD simulations, usually employing turbulence models [26], even for the case of internal cryogenic cooling [27]. Coolant penetration has mainly been studied by experimental means, where the coolant penetration is evaluated indirectly with the measured variables during cutting experiments, including tool wear, surface roughness, friction forces and temperatures. However, this implies that any coolant delivery parameters that could be optimised, are based solely on large amounts of experimental data.

Recently, designed textures have been employed on the rake or clearance surfaces of the cutting tool to modify the contact interface properties and the coolant function. In this case, the microchannels are formed because of textures in different shapes and sizes fabricated/allocated in the cutting tool. The contribution that these make to the machining process has been assessed with machining tests where the direction, location, size and patterns of the fabricated microchannels are varied significantly [28,29]. The results show that the friction on the tool-chip interface can be reduced with the application of surface-textured cutting tools, which in turn yields lower tool wear and an improved machinability [30,31]. Additionally, textured tools can also aid the chip breakage process [32]. Moreover, the texture alters the coolant's pathway due to the varying texture, which definitely alters the heat transfer and friction properties in the contact zone [33]. The effectiveness (e.g., how effectively they reduce friction and heat) of the microchannels mainly depends on their geometry and layout [34]. However, the shape and dimensions of the textures are designed with no systematic methodology and only selected by comparing vast amounts of experimental results. Thus, the effect of the texture on the coolant properties in the microchannels is yet to be understood in-depth.

Most of the research on coolant penetration is based on experimental work, while only little is related to deep understanding of the lubrication phenomena occurring in the cutting zone via modelling approaches. Thus, it is necessary to study the coolant penetration into the microchannels between the rough surfaces to reveal the mechanism of the microscopic lubrication phenomena in the cutting zone. This will enable more effective solutions for minimising friction and understanding the heat transfer mechanisms. In this paper, a comprehensive multiscale model is proposed to elucidate the scientific queries on the cooling and lubrication phenomena of coolant penetration into the microchannels in the tool-workpiece interface.

2. Definition of the problem

In a typical cutting process the coolant helps by reducing heat generation, friction and the adhesion tendency between the tool and the workpiece [35]. This results in a continuous chip (Fig. 1a), with the surface of the tool and the newly formed chip covered with a random structure filled with voids or spaces in between the rake face and the chip, which could be regarded as microchannels or microcavities (Fig. 1b). For enabling ease of understanding, this random structure can be simplified into a controlled network of microchannels on the tool's rake face, arranged in a woven pattern (Fig. 1c). The coolant delivered from the nozzle of the hydraulic system spreads into the large cavity formed by tool and the chip, with the coolant penetrating into the microchannels on the interface, where some of it is heated enough to vaporise (Fig. 1d). The coolant and the steam in the microchannels change the friction and heat transfer mechanism between the tool and the chip, which finally affects the cutting process.

3. Multiscale modelling of coolant penetration process

The cutting fluid applied during machining (Fig. 1) enters the wedge cavity formed by the varying chip and cutting tool. After filling up the cavity, the coolant will penetrate the contact zone between tool rake face and newly generated chip surface via microchannels. Therefore, a comprehensive multiscale analysis is needed to investigate the coolant penetration process. Thus, the whole analysis process is performed to deal with four problems, including the chip formation process, coolant delivery in the macro wedge cavity, coolant penetration into the microchannels and cooling/lubricating effect under high temperature and contact forces.

3.1. Constitutive and damage models for the cutting process and the chip formation process

The machining process is simulated with a Lagrangian-based 3D finite element model proposed in ABAQUS/Explicit as shown in Fig. 2. The Johnson-Cook constitutive model is employed to describe the plastic behaviour of the workpiece [36], which is made of Inconel 718. Therefore, the material flow stress in Eq. (1) is used to describe the strain and stress variation during machining [37]:

$$\overline{\sigma} = \left[A + B\overline{\varepsilon}^{n}\right]\left[1 + Cln\left(\frac{\dot{\overline{\varepsilon}}}{\dot{\overline{\varepsilon}}_0}\right)\right]\left[1 - \left(\frac{T - T_{room}}{T_{melt} - T_{room}}\right)^{m}\right] \quad (1)$$

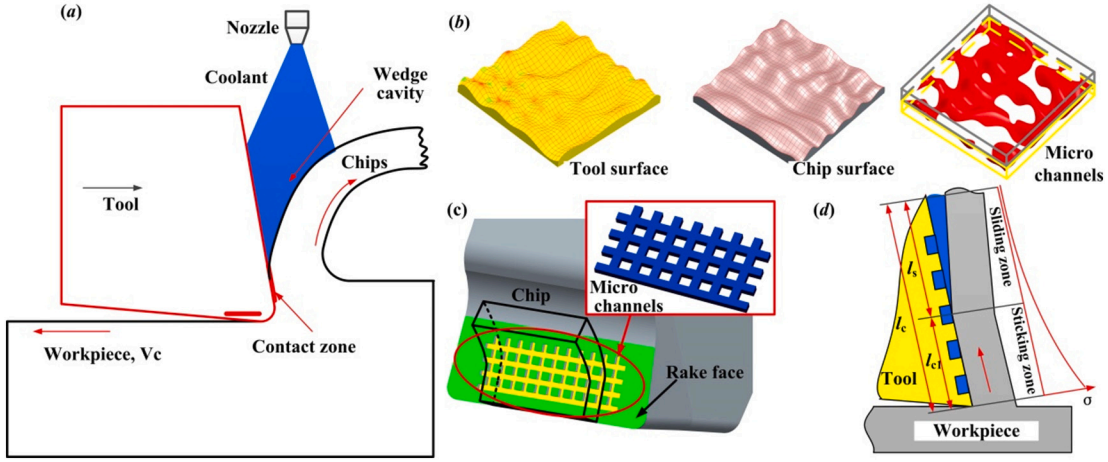

Fig. 1. Overview of the coolant penetration problem in the contact zone between cutting tool and workpiece. (a) General cutting process with coolant delivery at the tool-chip interface. (b) The rough surfaces of the tool and the chip allow for microcavities to be in place, which can be regarded as microchannels. (c) The microcavities are approximated with rectangular microchannels in a woven pattern. (d) Coolant penetration from the main large cavity and into the microchannels occurs in the contact zone, where some of the coolant is vapourised due to the elevated cutting temperatures.

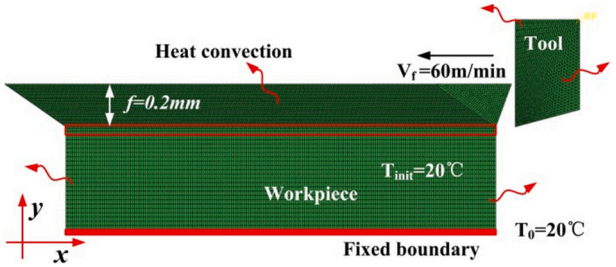

Fig. 2. FEM model for the machining process simulation. The Johnson-Cook constitutive and damage models for Inconel 718 were employed for the simulations.

where the equivalent stress is $\bar{\sigma}$, the yield strength of the workpiece material at room temperature is A, the hardening modulus is B, the coefficient dependent on the strain rate is C, the work-hardening exponent is n, the thermal softening coefficient is m, and ε denotes the equivalent plastic strain; refer to Table 1 for the specific values for each variable. T_{melt} and T_{room} represent the melting temperature of the material and room temperature, respectively. The strain to initial fracture is based on the Johnson-Cook damage model shown in Eq. (2), which evaluates the accumulated damage according to an energy evolution law in which the fracture occurs after the element's energy reaches the threshold value [38].

$$\bar{\varepsilon}^f = \left[D_1 + D_2 e^{D_3 \frac{\sigma_m}{\bar{\sigma}}}\right]\left[1 + D_4 ln\left(\frac{\dot{\bar{\varepsilon}}}{\dot{\bar{\varepsilon}}_0}\right)\right]\left[1 - D_5\left(\frac{T - T_{room}}{T_{melt} - T_{room}}\right)^m\right] \quad (2)$$

As shown in Fig. 2, the workpiece is fixed at the bottom. The cutting tool is assumed to be rigid and moving at constant cutting speed of 60 m/min. The workpiece and the tool are both meshed with quadrilateral plain strain elements. A mesh sensitivity study was iteratively performed until the final mesh size exerted insignificant changes to simulation outputs (e.g., forces, temperatures). The minimum element sizes of the workpiece and the cutter were finally set to be 0.001 mm and 0.002 mm, respectively. The main problems in the contact zone are the friction forces and heat transfer, and thus, a Coulomb model for friction was employed for calculating the friction forces. Then, it is assumed that the all the friction and plastic work during the machining process are converted into heat, which is transferred between the contact bodies mainly through conduction. Since the friction coefficient and the heat transfer coefficient rely on the contact pressure and distance away from the tool tip, a subroutine is developed to implement the changing law between these variable coefficients and the instantaneous pressure and distance. And then, the friction coefficient and heat transfer coefficient are updated according to the real contact status in every iteration. Beyond the contact zone, the heat is transferred into the surroundings mainly by convection with heat transfer coefficient of 20 W/m^2/°C. The initial temperature of workpiece and cutter and the room temperature are set as 20 °C. Following this, a transient coupled thermal analysis is executed to analyse the cutting process, which ultimately yields the cutting forces, temperature field and chip morphology.

3.2. Macro coolant flow modelling in the wedge cavity

The coolant enters the wedge cavity (Fig. 3a) and interacts with both tool and chip surfaces. Due to the impact that the fluid has on the process, its properties must be known precisely; therefore, these can be obtained with the Computational Fluid Dynamics (CFD) model shown in Fig. 3b. The CFD's solution volume is formed by the tool rake face, the chip surface (on the rake face side), the nozzle and its surrounding atmosphere. The nozzle is considered as the fluid inlet with a constant velocity, which is calculated with the nozzle geometry and the coolant supply system. The rake face of the tool, the chip surface and the nozzle pipe are treated as stationary non-slip walls. The side surfaces are treated as pressure outlets with atmosphere pressure. The interaction between the air and the coolant is described by a multiphase Volume of Fluid (VOF) model with k-ε fluid characteristics.

In the simulation, the pressure of the coolant is set to 5.5 MPa, which corresponds to a velocity at the nozzle outlet of 105.6 m/s. Following this, a steady analysis is performed to get the pressure (Fig. 4a) and the velocity field (Fig. 4b) of the coolant in the wedge cavity. The pressure

Table 1
Parameters for the Johnson-Cook constitutive and damage models for Inconel 718 [39].

A/MPa	B/MPa	n	C	m	$\dot{\bar{\varepsilon}}$/s^{-1}	T_{melt}/°C	T_{room}/°C	D_1	D_2	D_3	D_4	D_5
1262	1354	0.5	0.006	1.08	0.001	1340	25	0.4058	0.750	−1.450	0.04	0.89

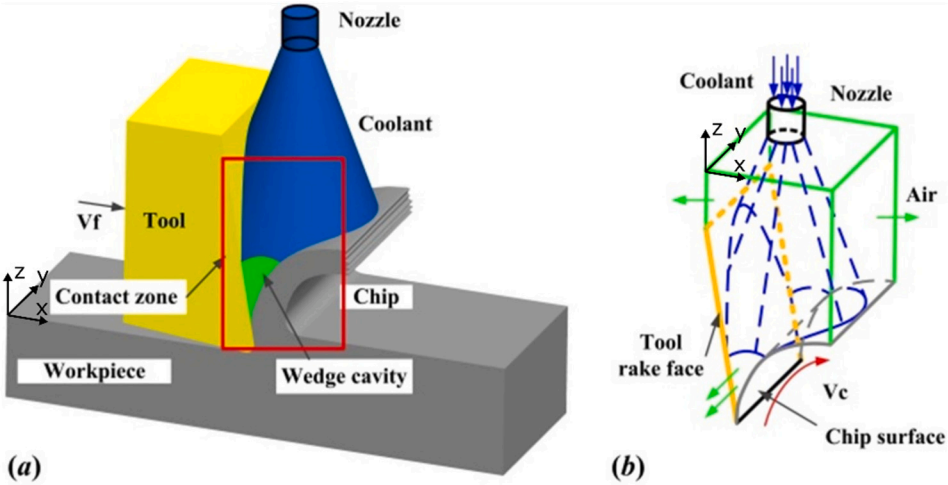

Fig. 3. Analysis of coolant flow in the macro wedge. (*a*) Macro wedge cavity. (b) Boundary conditions for multiphase VOF CFD model.

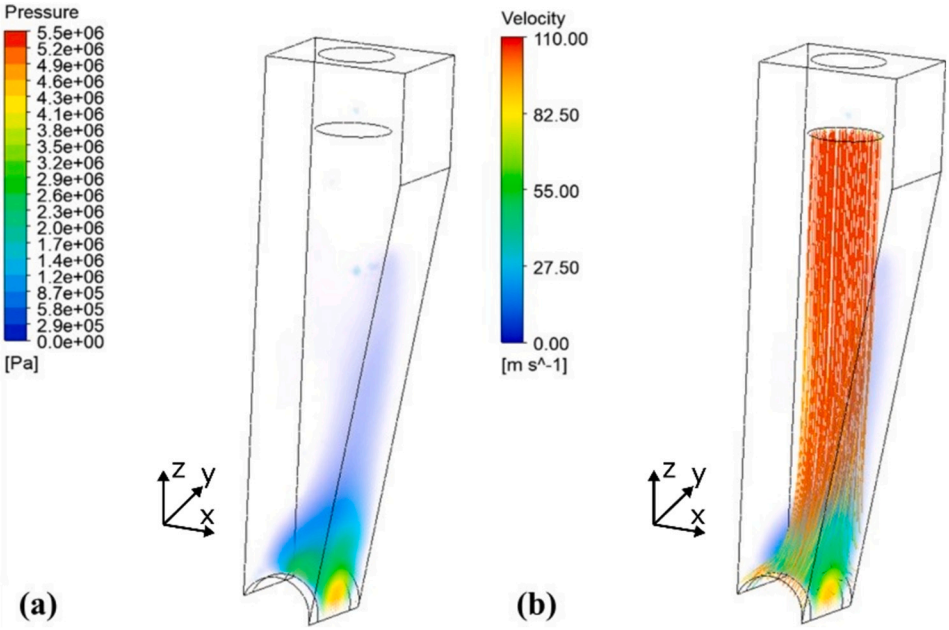

Fig. 4. Simulated results of coolant properties in the macro wedge. (a) Pressure field. (b) Velocity field.

on every node at the end of the wedge cavity is obtained as a function of the cutting width, *y,* by fitting the discrete values with a second order polynomial expression (Fig. 5), described by Eq. (3).

$$P_{min} = -3.0226 \times 10^{12} y^2 + 5.3191 \times 10^6 \tag{3}$$

3.3. Micro penetration model of coolant in the microchannels

The microchannels between the tool's rake face and the chip permit the coolant from the outlet of the wedge cavity to enter the contact area. The coolant flow is affected by the channel morphology, contact pressure and thermal boundaries. The coolant properties are defined not only by the inlet pressure, the temperature and relative velocity of the tool and the chip, but also by the air in the channels and the steam generated by the coolant that is evaporated due to heat. Hence, a thermal and multi-phase CFD model is built to study coolant flow in the microchannels (Fig. 6), considering the pressure distribution (as shown in Fig. 5) and the transient nature of the process. A k-ω viscous turbulence model [26] is selected to achieve enough accuracy both near the wall and in the channels. Three phases are defined, including air, steam, and coolant, with the phase change of coolant to steam described by the evaporation-condensation mass transform model. Initially, the volume is filled with air, but then, the coolant is introduced at the entrance. The simulation is executed after setting appropriate parameters to obtain the fluid properties, including the volume fraction, velocity, pressure and temperature field of all three present fluids (i.e., coolant, steam and air), as shown in Fig. 7. In this case, the heat transfer coefficient h_{lij} at node (*i*, *j*) of the coolant-solid interface can be obtained with Eq. (4):

$$h_{lij} = \frac{q_{ij}}{\Delta T_{ij}} \tag{4}$$

where, q_{ij} is the heat flux at node (*i*,*j*) and $\triangle T_{ij}$ is the temperature increment of node (*i*,*j*) relative to the rake face. An example of this is shown in Fig. 7c.

3.4. Lubrication and heat transfer modelling in the contact zone

Friction coefficient and heat transfer coefficients are the two most

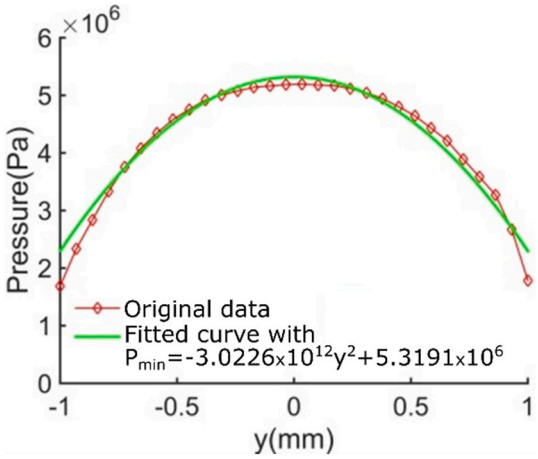

Fig. 5. Pressure distributions of coolant at the entrance of microchannels. The original data is shown, as well as the fitted curve with Eq. (3).

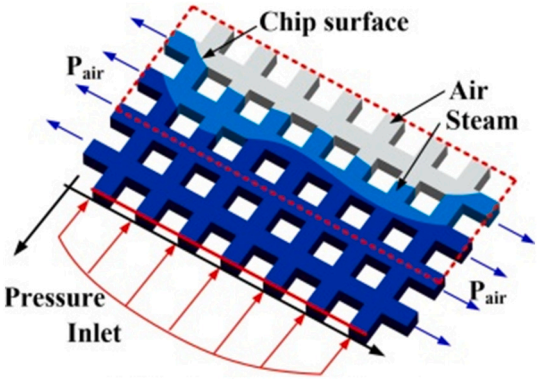

Fig. 6. Boundary conditions for the coolant flow analysis in the microchannels.

relevant parameters for introducing the effect of coolant in the contact zone during the machining process (Fig. 8a). The heat is transferred between the tool and the workpiece by both the coolant-solid and solid-solid interfaces. The heat transfer coefficient of the coolant-solid interface (h_{li}) is obtained with Eq. (4) and the heat transfer coefficient of the solid-solid interface (h_{sj}) is calculated with a thermal conductance analysis of the surface (taking into account the morphology) and the applied load. Following this, the total heat transfer coefficient is obtained by combining the interfaces in a parallel sequence, as shown in Fig. 8b and in Eq. (5).

$$h = 1 \Big/ \sum_{i,j} \left(\frac{1}{h_{li}} + \frac{1}{h_{sj}} \right) \tag{5}$$

The friction force in the contact zone is obtained by two different methods according to the force distribution (Fig. 8b). In the sticking zone, the solid-solid interface friction coefficient (μ_{ss}) is assumed to be constant as it is difficult for the fluid to penetrate when the chip and the tool keep in constant contact under a large pressure. In the sliding zone, on the other hand, the friction force is heavily affected by the lubricating action provided by the coolant. Therefore, the lubrication problem can be described with a full film lubrication model (Fig. 8c).

The friction coefficient μ_l is obtained with the pressure distribution of the coolant film by solving the Reynolds equation (Eq. (6))

$$\frac{\partial}{\partial x}\left(\frac{\rho h^3}{\eta}\frac{\partial p}{\partial x}\right) + \frac{\partial}{\partial y}\left(\frac{\rho h^3}{\eta}\frac{\partial p}{\partial y}\right) = 6V_{chip}\frac{\partial(\rho h)}{\partial x} + 12\frac{\partial(\rho h)}{\partial t} \tag{6}$$

where h is the film thickness, η is the viscosity and V_{chip} is the relative velocity.

The solution of Eq. (6) is obtained with a finite difference method. Firstly, the lubrication film is meshed into $N_x \times N_y$ elements with intervals dx and dy in two directions. All the parameters are converted into a dimensionless format, where $dX = dx/L_x$ and $dY = dy/L_y$ are the dimensionless element sizes in x and y, respectively; $H_{ij} = h_{ij}/h_{out}$ is the dimensionless film thickness, and $P_{ij} = p_{ij}h_{ij}/\eta V_{chip}L_x$ is the dimensionless pressure. Then, the pressure at node (i, j) can be calculated with a second-order discrete formulation (Fig. 8d):

$$\begin{cases} F_{ij}\overline{P}_{ij} = A_{ij}P_{i,j+1} + B_{ij}P_{i,j-1} + C_{ij}P_{i+1,j} + D_{ij}P_{i-1,j} + E_{ij} \\ A_{ij} = \dfrac{H^3_{i,j+0.5}}{dY^2}, B_{ij} = \dfrac{H^3_{i,j-0.5}}{dY^2} \\ C_{ij} = \dfrac{H^3_{i+0.5,j}}{dX^2}, D_{ij} = \dfrac{H^3_{i-0.5,j}}{dX^2} \\ E_{ij} = \dfrac{\left(H_{i+1,j} - H_{i-1,j}\right)}{2dX} \\ F_{ij} = \dfrac{\left(H^3_{i+0.5,j} + H^3_{i-0.5,j}\right)}{dX^2} + \dfrac{\left(H^3_{i,j+0.5} + H^3_{i,j-0.5}\right)}{dY^2} \end{cases} \tag{7}$$

The equations for pressure in all nodes are derived with Eq. (7), and boundary conditions are applied at nodes which are on the surrounding edges. A program is developed to calculate the pressure distribution in the film via an iterative method. With this, the friction coefficient in the sliding zone (μ_l) can be obtained with Eq. (8).

$$\mu_l = \frac{\sum_{j=1}^{Ny}\sum_{i=1}^{Nx}\left(\frac{0.5h_{ij}\left(p_{ij}-p_{i-1j}\right)}{dx} + \frac{V_{chip}\eta}{h_{ij}}\right)dxdy}{\sum_{j=1}^{Ny}\sum_{i=1}^{Nx}p_{ij}dxdy} \tag{8}$$

4. Experimental setup

Different kinds of orthogonal turning tests are performed in a laboratory setup (Fig. 9a) to obtain the cutting forces and cutter temperature when coolant and different inserts are applied. The insert (SECO 150.10-3N-12) is characterised by a 0° rake angle and 6° clearance angle. Two types of inserts are employed, with one being original without any microchannels on the rake face, and the other one modified with laser machining to possess several crossed microchannels with a square cross section on the rake surface (Fig. 9b). In the past, laser texturing has also been explored for enabling a chip breakage mechanism [32]; however, here the laser texturing is aimed at creating the microchannels on the rake face to act as a fluid delivery system. Hocut 3380, which is a water-based fluid with ca. 90–92 % water content is chosen as coolant and delivered to the cutting area by holes inside the blade at 5.5 MPa. Several disks with 2 mm thickness and 4 mm spacing were previously machined on an Inconel 718 cylinder to prepare the sections for the orthogonal turning tests. During machining, the temperature of the insert is measured with a thermocouple (Type K) embedded under the insert's rake face near the cutting zone (Fig. 9c), while a dynamometer (Kistler 9121) is employed to capture the cutting forces. In the experiments, the feed rate is set to 0.2 mm/rev, the cutting speed is kept constant at 60 m/min, and a fixed length of 6 m was cut for each test. To study the role of the microchannels upon the coolant delivery, the experimental trials were done under coolant-applied conditions, thereby providing a straightforward assessment between the two types of inserts (flat and channelled, respectively). At the end of the experimental trials, the surface morphology of both the disks and the inserts were scanned with a 3D surface profile measuring instrument (Alicona G4) to assess the surface topography for each machining condition.

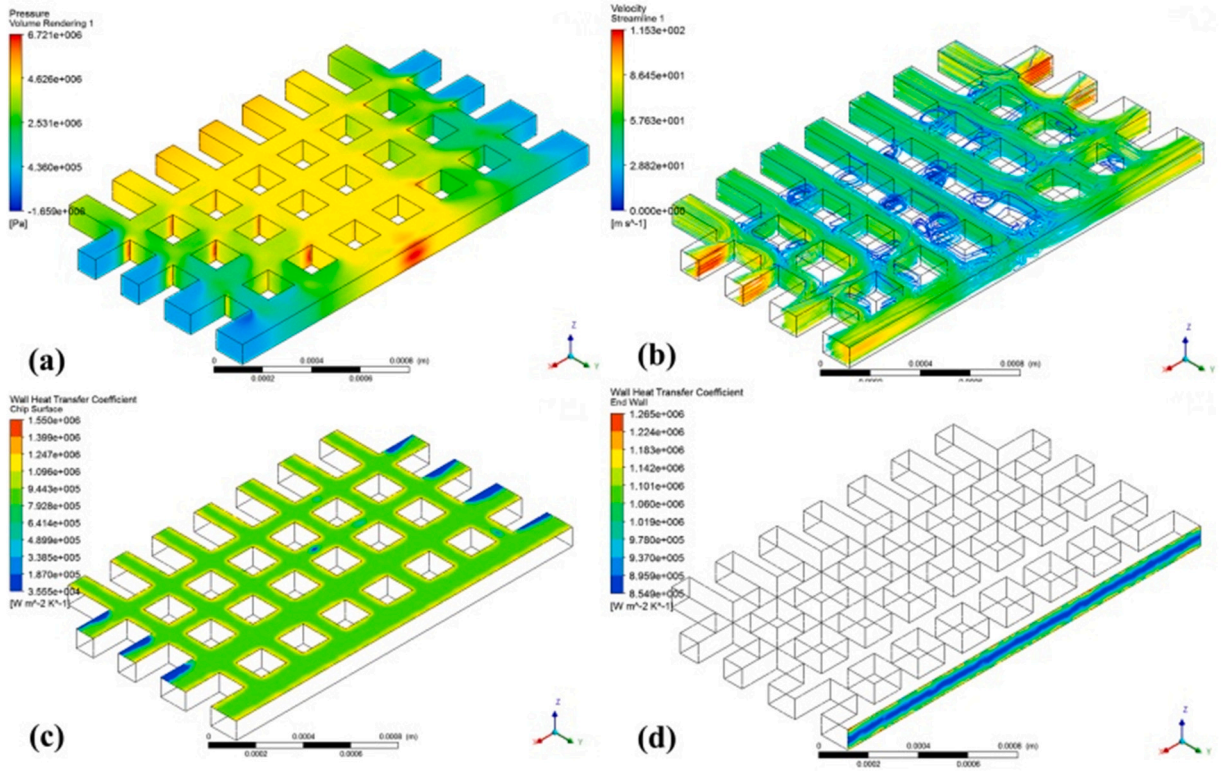

Fig. 7. Simulated results of coolant properties in the microchannels. (a) Pressure. (b) Velocity. (c). Heat transfer coefficient on the rake face. (d) Heat transfer coefficient on end surface.

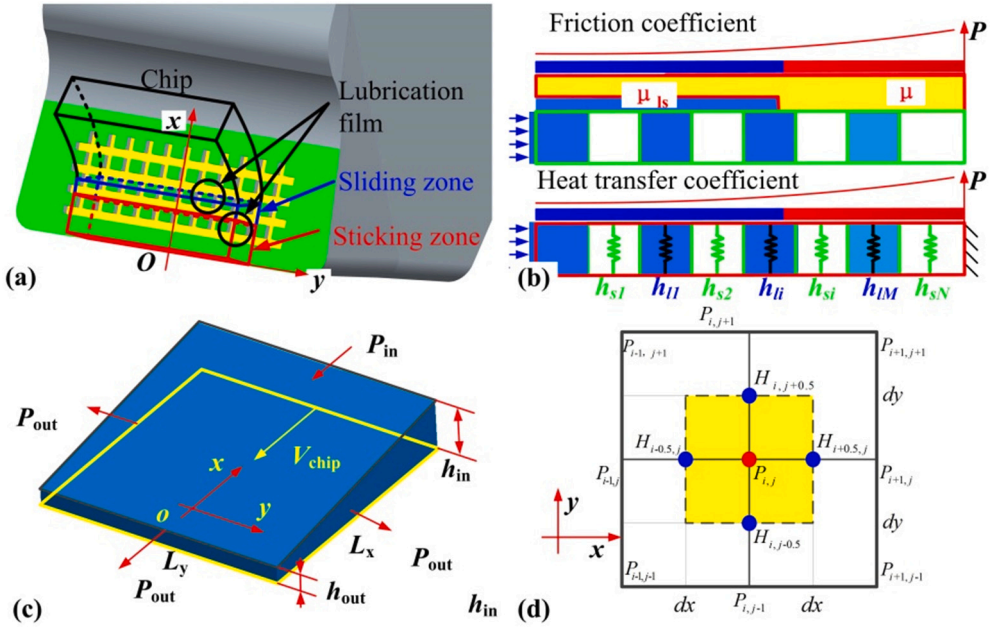

Fig. 8. Lubrication model at the interface: (a) Coolant distribution in the sticking and sliding zone. (b) Friction coefficient and heat transfer coefficient model in the contact zone. (c) Boundary conditions for lubrication film. (d) Mesh grids and discretized scheme for film model.

5. Results and discussion

5.1. The role of the microchannels upon the contact status on rake faces

The wear condition on the rake surface of the different inserts after machining are shown in Fig. 10. In the presence of coolant, the flat insert presents a regular uniform wear along the cutting edge (Fig. 10a) that is only present at small depths (ca. 124 μm); this is to be expected due to the presence of coolant during the machining process. Interestingly, however, the channelled insert (Fig. 10b) presents a significantly larger depth at which wear is detected (ca. 405 μm), an aspect which might be initially not expected due to the enhanced coolant delivery but could be explained by the stiffness of the tool's edge. Since the microchannels were fabricated via laser processing near the cutting edge (see Fig. 9b),

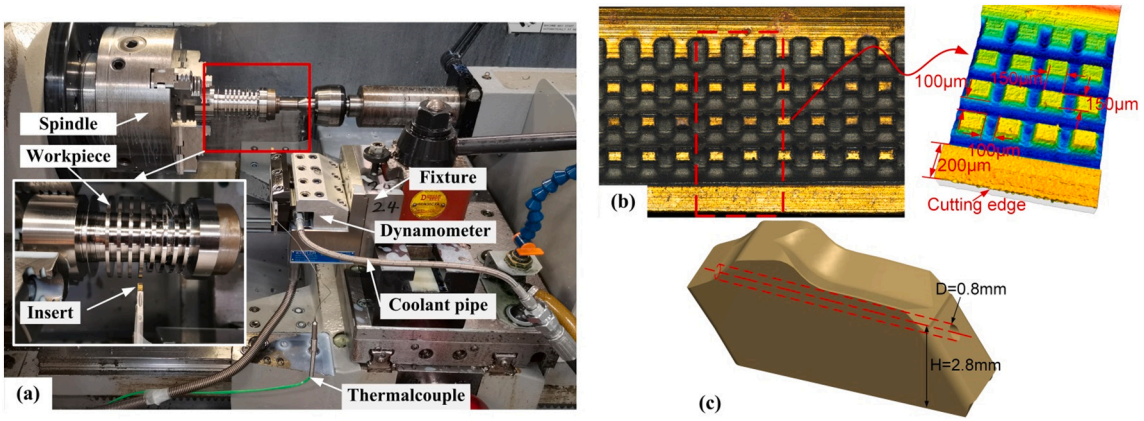

Fig. 9. Experimental setup employed for the orthogonal turning process. (a) Testing setup. (b) Fabricated microchannels in the insert. (c) EDM hole in the insert for thermocouple insertion.

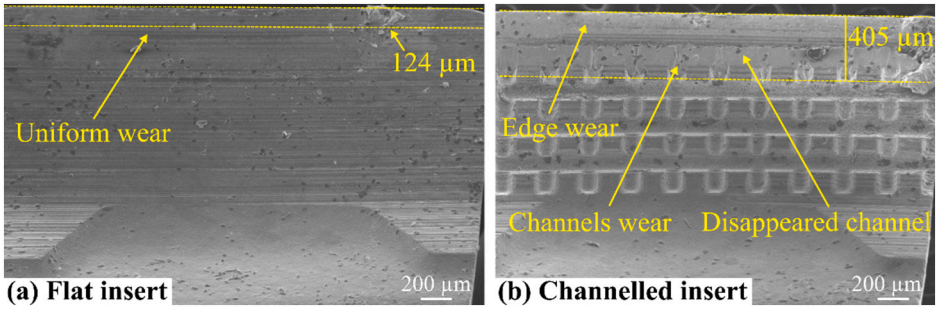

Fig. 10. SEM inspection of the inserts' rake faces following machining under coolant conditions. (a) Flat insert, depicting a minimum amount of wear that is constrained to about 124 μm from the cutting edge. (b) Channelled insert showing a larger depth of wear (405 μm) due to the reduced stiffness and the increased friction in the contact zone with the microchannels.

this implies that the stiffness of the edge is drastically reduced due to the absence of material. Since the depth of cut is 200 μm, and this is in-line with the depth at which the microchannels' first row is located, it would be expected that the maximum bending stress would occur at the microchannels locations, thereby enabling ease of deformation. Additionally, since the chip flow would be in contact with the sharp edges of the microchannels, these ones will be also prone to deformation due to the constant rubbing against the chip in the contact zone, instead of enabling the non-hindered flow that the flat insert offers. Another way of analysing this phenomenon is that the microchannels could be regarded as surface anomalies or defects from the pristine cutting tool shape (i.e., due to the changes in height generated by the microchannels), and it is well known that surface defects lead to accelerated wear mechanisms [40]. This is the reason why the first row of microchannels disappears (i.e., smears out) and produces the much larger wear depth.

The deformation of the rake face geometry during machining has a great effect on the accuracy of workpiece, since a straightforward correlation between the insert's morphology and the machined surface exists. For instance, the workpiece surfaces (Fig. 11) clearly show that there is a match between their morphology and the respective shapes

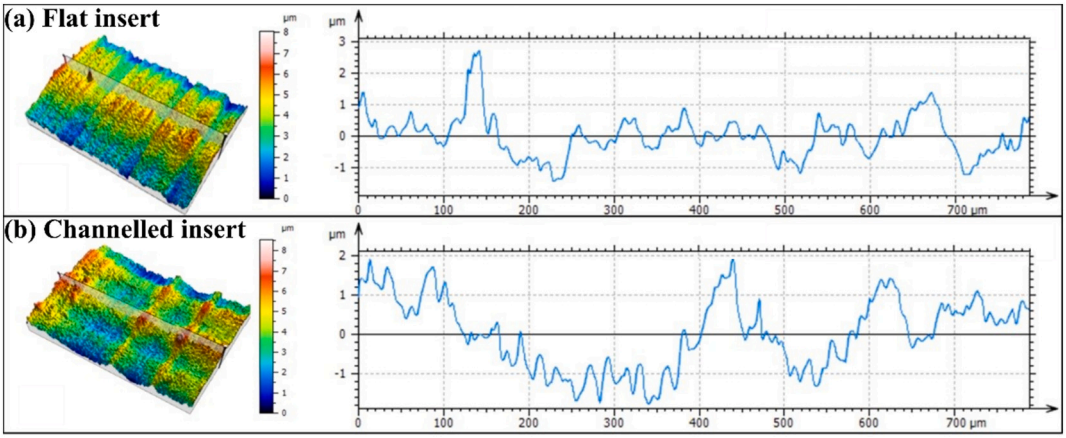

Fig. 11. Surface morphology of the machined workpieces following machining under coolant conditions. (a) Surface produced with the flat insert, where a cross sectional analysis yields a roughness between −1 μm and 1 μm. (b) Surface produced with the channelled insert, where a slightly larger roughness is depicted (variation between −2 μm and 2 μm).

from their corresponding inserts shown in Fig. 10. Due to the fluid presence, in both cases the machined surface is considerably smooth. However, due to the lower tool wear, the flat insert produced a smoother surface (Fig. 11a), as opposed to the slightly rougher surface produced with the channelled insert (Fig. 11b).

As explained previously, the contact area between the insert's rake face and the workpiece is composed of a sticking zone and a sliding zone. The length of the contact zone can be assessed by measuring the distance between the tool tip and one particular position on the rake face where the contact pressure changes from positive values to almost zero (example shown in Fig. 12a); experimentally, this was achieved by examination of the rake face at the end of each machining test with a 3D surface profile scanner (Alicona G4). The contact lengths for the different inserts are shown in Fig. 12b, where it is easy to note that the simulation results are similar to the experimental ones. It is interesting to see that both the simulations and the experimental measurements show an insignificant difference between the flat insert and the channelled insert. Nevertheless, the standard deviation obtained experimentally is significantly larger for the channelled insert than for the flat one. The reason for this is the presence of the microchannels, which due to accelerated wear enable a larger variation on the mean values of contact length.

5.2. The role of the microchannels upon cutting forces and friction

The measured specific cutting and thrust forces are shown in Fig. 13, where it is easy to see that the channels themselves can bring the benefit of decreasing the machining forces when compared to the flat insert. The specific cutting force for the flat insert is steadily constant, with an average value of 403 N/mm (Fig. 13a), which sees a significant reduction of 8.5 % produced by the microchannels (specific cutting force of 369 N/mm), as it can be seen in Fig. 13b. However, note how the force depicts a slightly decreasing trend as a function of time. The specific thrust forces for the flat insert (Fig. 13c) show an increasing trend between 50 N/mm and 100 N/mm, producing an average value of 70.5 N/mm. This value is remarkably reduced by the microchannels (Fig. 13b), which are 26.6 % lower in mean value, plus also show a slightly decreasing trend (i.e., instead of the increasing trend from the flat insert). Since the friction force runs along the rake face (i.e., 90° respect to the cutting direction), the chip flow will be drastically affected along this direction, which is why the sensitivity of the microchannels is more easily noticeable in the thrust force direction.

The mean specific cutting and thrust forces of experimental measurements and simulations are compared in Table 2, also including the friction coefficient. Both in simulations and in experimental measurements, the microchannels generate a lower value of forces and of friction coefficient, aspect that is due to the enhances coolant delivery near the cutting zone. While the cutting and thrust forces can be reduced by 8.5 % and 26.6 %, respectively, the friction coefficient also is lower by 19.8 %, changing from being 0.175 for the flat insert and 0.140 for the channelled insert. Interestingly, however, is that while the simulations also show the benefit of the microchannels (i.e., they also produce less values of force and friction in the presence of the microchannels), they are significantly different than the experimental results (see Table 2). The reason for this disparity could rely on the fact that the model does not consider the wear of the insert, which is enhanced by the existence of the channels. Since the channels rapidly wear out, less chip material gets trapped within the channel cavities along the rake face and therefore the chip flow eases up along the thrust force direction. However, the cavities being worn out is not considered in the model, and thus, the model yields a significantly larger mean value of thrust force (Table 2) because of more chip volume being trapped within the cavities during the chip flow. This error is much less in the cutting forces, where due to the wear, a ploughing effect could more easily be enabled experimentally, thereby producing slightly larger experimental values than simulated ones. These results highlight the important role that the microchannels have upon coolant delivery during the machining process and that they are efficient for decreasing cutting and thrust forces, but also show that there is a need to consider tool wear in the modelling process.

As previously stated, the channelled inserts show a gradually decreasing trend over time (see Fig. 13). This is an interesting phenomenon that occurs due to the ongoing engagement of the sharp edges of the channels during the cutting process (see Fig. 14). During the cut, the channels' sharp edges aid in the cutting process by making a series of small cuts in the chip, which could in turn act as stress concentrators that end up yielding lower stresses along the shear plane to produce the cut. Nevertheless, this in turn would be accompanied with accelerated tool wear in the microchannels, especially those closest to the cutting zone, an aspect that is validated with the tool assessment post-machining (Fig. 10b), in which the first row of microchannels has disappeared due to the ongoing contact with the chip.

5.3. The role of the microchannels upon cutting temperatures

Based on the previous section, it has been proved that the enhanced coolant delivery through the microchannels can have a significant impact upon the lubrication effect. However, there is still the need to understand the cooling effect it may incur during the machining process. For this, the measured variations of temperature on the setting point inside the insert (see Fig. 9c) were compared for both inserts (Fig. 15). The temperature produced by the flat insert reached a maximum of 41.2 °C, which can be reduced by 13.3 % (i.e., decreasing to 35.7 °C) if

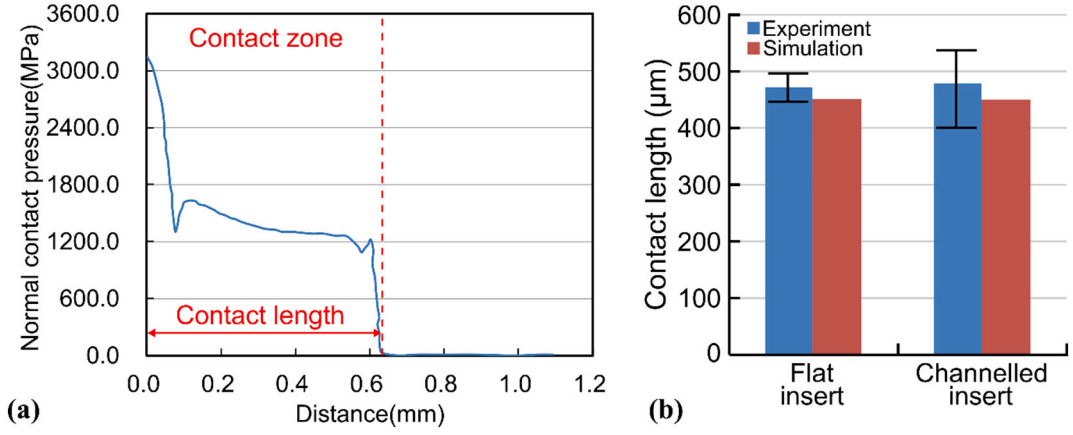

Fig. 12. Contact pressure and contact length on the rake face. (a) Example of the contact pressure for the flat insert without coolant. (b) Comparison of experiment and simulation results of contact length on the rake face during machining for both cutting inserts and under coolant conditions.

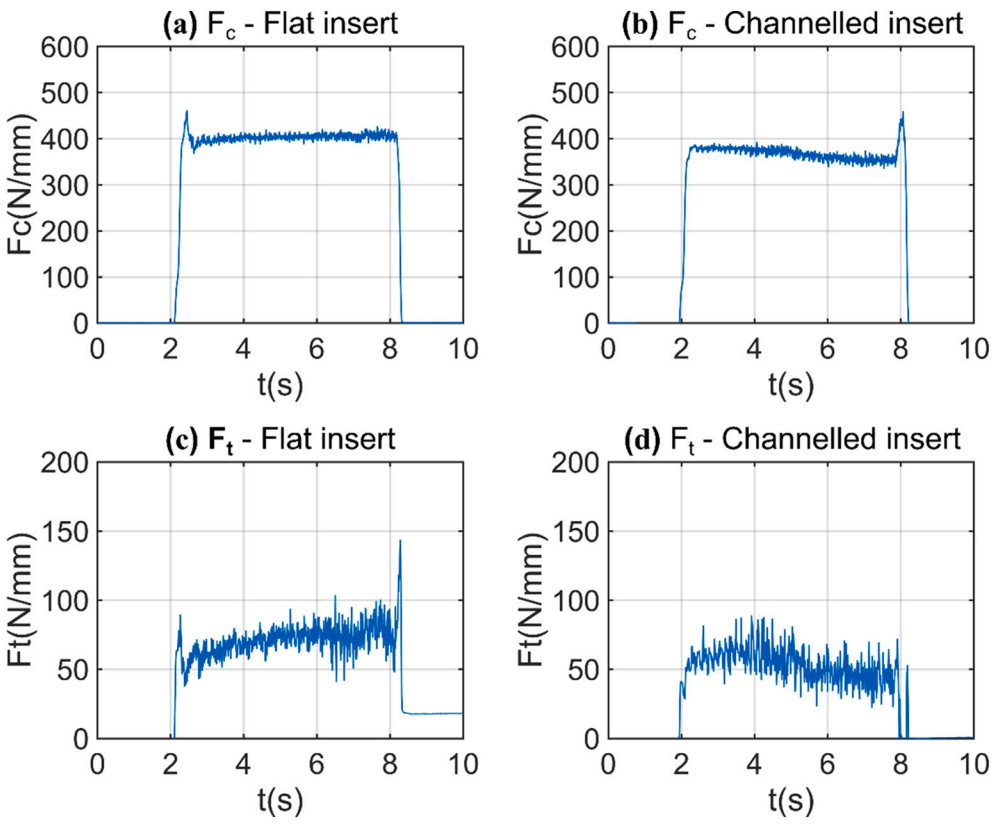

Fig. 13. Measured specific cutting and thrust forces for the different inserts during machining. (a) The specific cutting forces from the flat insert depict a constant trend of 403 N/mm. (b) The channelled insert produces a slightly smaller specific cutting force of 369 N/mm in average but showing a decreasing force trend. (c) The thrust forces from the flat insert show an increasing trend between 50 N/mm and 100 N/mm, producing an average value of 70.5 N/mm. (d) The channelled insert produces a decreasing thrust force trend of 52 N/mm in average.

Table 2
Comparison of specific cutting force, specific thrust force and friction coefficient from the experimental trials and the simulations.

	Specific cutting force			Specific thrust force			Friction coefficient		
	Flat insert (N/mm)	Channelled insert (N/mm)	Difference	Flat insert (N/mm)	Channelled insert (N/mm)	Difference	Flat insert	Channelled insert	Difference
Experiment	403.5	369.1	−8.5 %	70.5	51.7	−26.6 %	0.175	0.140	−19.8 %
Simulation	350.0	326.0	−6.9 %	120.0	109.0	−9.2 %	0.343	0.334	−2.5 %
Error	−13.3 %	−11.7 %		70.2 %	110.7 %		96.2 %	138.5 %	

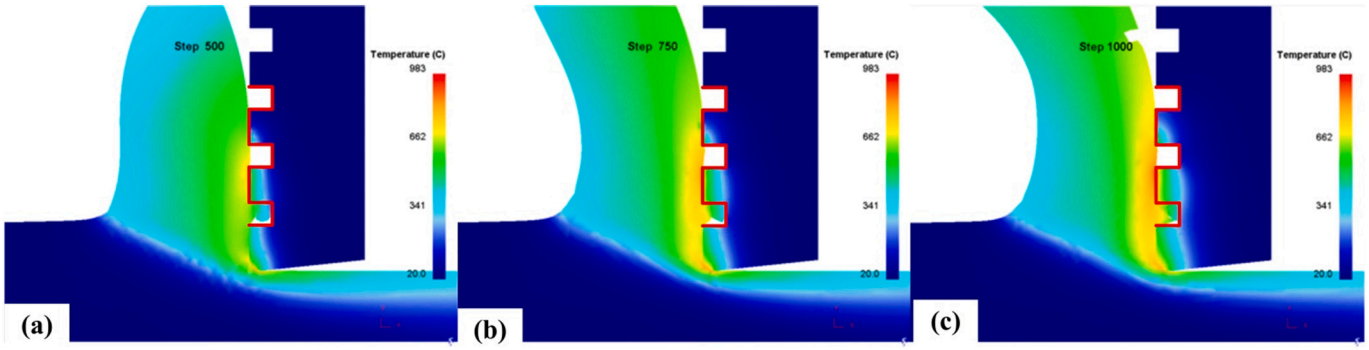

Fig. 14. Simulated cutting processes for the channelled insert with coolant delivery at different time steps: (a) Step 500. (b) Step 750. (c) Step 1000. Note that the microchannels produce an enhanced cutting mechanism in which these points of contact act as micro-cutters or stress concentrators.

the microchannels are considered in the tool.

Since the temperatures shown in Fig. 15 are constrained to the point of measurement within the inserts (i.e., they do not measure the temperature in the cutting interface but slightly beneath the rake face), simulations were also completed to find out the thermal fields in the tool-workpiece interface (see Fig. 16), where it is easy to note that much higher temperatures can occur near the cutting zone. While the flat insert yields a temperature (i.e., as measured beneath the rake face) of 41.2 °C (see Fig. 15), the simulation shows that at the cutting interface, the maximum temperature is ca. 947 °C (see Fig. 16a) which is about 23 times larger. In the case of the channelled insert, the maximum temperature in the cutting interface is approximately 750 °C (see Fig. 16b),

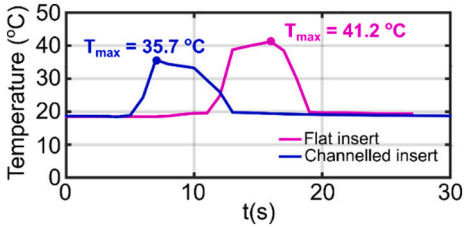

Fig. 15. Measured temperatures under the rake face for the flat (magenta colour) and the channelled (blue colour) insert. (For interpretation of the references to colour in this figure legend, the reader is referred to the web version of this article.)

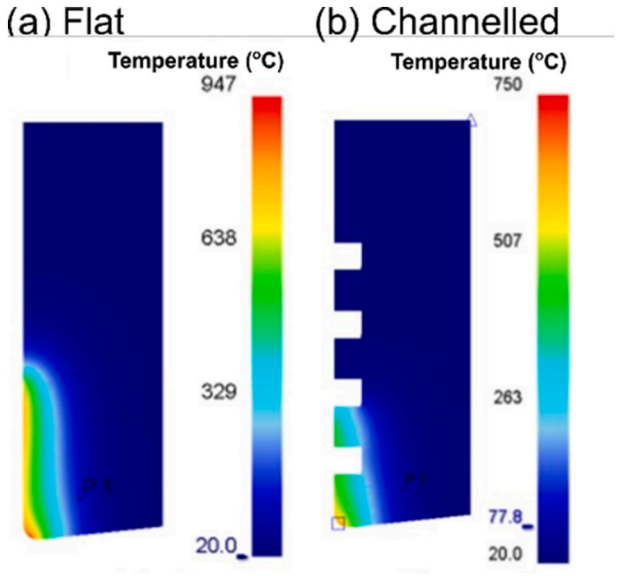

Fig. 16. Temperatures fields of the two inserts at steady state during machining with coolant conditions. (a) The flat insert with coolant yields a maximum temperature of 947 °C. (d) However, the microchannels manage to make a reduction in temperature (750 °C), which shows the capability of the channels towards heat dissipation.

which is, similarly, about 21 times larger than the measured temperature of 35.7 °C beneath the rake face (see Fig. 15). The significant difference between the temperatures at the rake face and then slightly beneath (i.e., at thermocouple location) is justified by the role of the coolant and the contact length. Based on the simulation, the spatial distribution range of the temperature will be smaller because of the contact length reduction that the channels create. Consequently, heat dissipation via diffusion into the insert's body is hindered. This implies that most of the heat will be concentrated in the contact zone near the cutting edge; thus, the thermal readings beneath the insert's rake face are much lower than those at the interface. Additionally, according to the simulation, there is a 20.8 % reduction in maximum temperature when the channelled insert is employed. This implies that coolant delivery is significantly improved by the microchannels, even if this hinders the heat diffusion into the tool. These simulation results are in line with those measured experimentally (Fig. 15), highlighting that in regions closer to the cutting edge of the tool, the difference between the temperatures can be more drastic.

5.4. The role of the microchannels upon chip morphology

It is known that chip analysis can revel significant information about the influence of the workpiece's texture [41,42] and the resultant surface integrity [43]. Thus, chips were collected from the turning tests for examination, towards assessment of the surface integrity, which in turn, should reflect the coolant penetration status (see Fig. 17). An enhanced chip fragmentation can be seen during the cutting process where a long chip (Fig. 17a) is generated with a flat insert, while the coolant makes this breaking process more effective (Fig. 17b). This is due to the coolant pressure and enhancement of fluid delivery through channels which leads to a reduction of the chip-tool contact length while also tends to break the chip. To quantify the chip geometry, the degree of chip segmentation (G) is defined as $(H_{max}\text{-}H_{min})/H_{max}$, where H_{max} and H_{min} are the maximum and minimum chip thickness respectively [44]. Under coolant conditions, the flat insert produced a segmentation of $G = 0.500$, only to see a 10.9 % reduction due to the microchannels ($G = 0.446$), which is line with the lower friction coefficient that this insert produces (refer to Table 2). Nevertheless, it is necessary to understand what this might imply in terms of the localised shearing taking place within the chip, which is why zoomed-in portions of the chip are shown in Fig. 17c, d, where a similar thin white layer exists for both inserts with the main difference being that the chip produced with the channelled insert (Fig. 17d) possesses an increased shear banding per segment, if compared to the flat insert chip (Fig. 17c). The results indicate a distinct cooling/lubricating effect between the chip and the tool, which results in lower normal and shear stresses in the chip-tool interface. This, on the other hand, proves the advantage of the channels in terms of a more efficient coolant delivery.

6. Conclusions

This paper proposes a multiscale comprehensive theoretical model for the coolant penetration into the microchannels at the interface between tool and workpiece for the case of orthogonal cutting with a cooling system enabled. Both simulation and experimental studies have been performed to study the effect of coolant and lubrication mechanisms on the machining process of Inconel 718.

- A multiscale mathematical model was developed in order to predict cutting forces and temperatures during machining, while considering coolant delivery through microchannels embedded on the cutting inserts. This was achieved by employing a Johnson-Cook constitutive and damage model to describe the flow stress and threshold strain for Inconel 718. A CFD analysis was coupled with this to calculate the pressure distribution along the cutting width of the fluid. Then, the pressure was utilised in a micro-penetration model of the coolant into the wedge cavities (i.e., the microchannels on the insert) using a A k-ω viscous turbulence model, taking into account the phase change of the coolant into steam near the cutting zone and through the channels. Finally, the heat transfer coefficients and localised friction values were calculated for the solid-solid and solid-coolant interfaces within the sliding zone of the chip.
- The proposed multiscale comprehensive model has been well verified by comparing with experimental results and revealed that the cooling effect principle of the coolant is enabled by changing the heat transfer coefficient, while the lubrication mechanism is enabled by changing the friction coefficient on the micro-contact surfaces. The cooling and lubricating effect of the coolant is determined by the flow properties, microchannels geometry and cutting parameters. Nevertheless, it is also noted that is necessary to include tool wear in the model to account for the tool deformation along the cut, which is of great relevance when dealing with such a localised analysis (i.e., in the tool-chip interface).
- The cooling and lubrication mechanisms have an important influence on the whole machining process but vary in degree of contribution on the different machining parameters or characteristics. The cooling mechanism of the coolant has a direct effect on dramatically decreasing temperature and the spatial range of the thermally affected zone by enhancing heat dissipation from the workpiece and

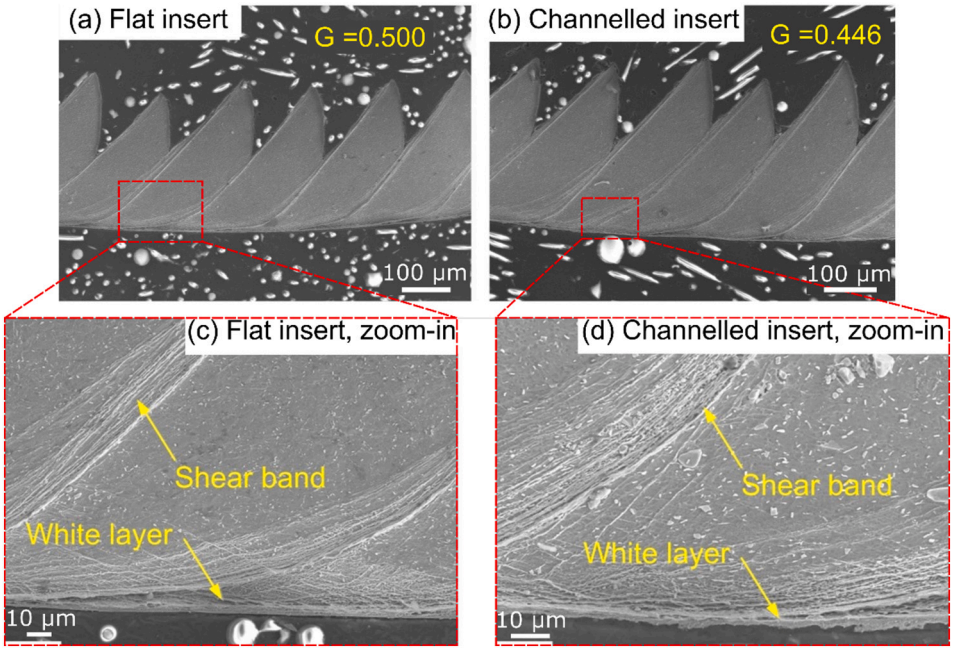

Fig. 17. Chip morphologies produced with the different inserts under coolant-applied machining conditions. (a) The flat insert with produced a degree of chip segmentation of $G = 0.500$. (b) The channelled insert produced $G = 0.446$, i.e., a 10.9 % reduction. (b,c) A zoomed-in view of the chip enables to visualise the shear bands and the white layer within the chip. In both cases, the white layer is essentially of the same thickness, with the only difference between the chips (besides the segmentation) being that more shear bands appear per segmentation with the channelled inserts.

insert to the coolant. And the two mechanisms (lubrication and cooling) both work in the contact zone, which leads to a significant reduction of the contact length, friction coefficient and cutting and thrust forces.

- The textured tool benefits the cutting process by reducing the contact length, cutting forces and friction coefficient. However, the micro-channels contribute only little on the reduction of temperature due to the shortage of a heat dissipation mechanism (i.e., diffusion is hindered due to the discontinuities in the material formed by the microchannels). Nevertheless, the microchannels aid the coolant on entering the contact zone, which helps to overcome this problem. However, it should be noted that fabrication of channels on the rake face will reduce the strength of cutting edge and break the coating layers integrity. Inappropriate design will greatly increase wear and friction which will result in cutting edge damage. The effectiveness of the microchannels depends mainly on their layout and dimensions. Thus, a systemic design methodology for the microchannels is needed to further increase their effectiveness.
- As shown by this work, the modelling process is quite intricate due to the multiscale necessity for coupling the macro-level fluidic and machining conditions with the micro-level contact conditions between the coolant, the tool, and the workpiece. However, it was shown that tool wear is significantly important and thus could comprise a future line of research in the topic of customised textured tools for improved machining performance. It is expected that this research topic enhances predictive models for tool life and machining behaviour, and extends also to other type of cooling methods such as cryogenic cooling (e.g., CO_2 or LN_2).
- The present results have not only revealed the fundamental mechanism of the coolant in the cutting zone, but also are very useful for the development of novel cooling methods and improved tool design.

Declaration of competing interest

The authors declare that they have no known competing financial interests or personal relationships that could have appeared to influence the work reported in this paper.

Acknowledgements

The authors thank the Nanoscale and Microscale Research Centre (nmRC) for providing access to instrumentation.

Funding

The authors acknowledge the support from the National Natural Science Foundation of China (Grant No. 51975302).

References

[1] Kaminski J, Ljungkrona O, Crafoord R, Lagerberg S. Control of chip flow direction in high-pressure water jet-assisted orthogonal tube turning. Proc Inst Mech Eng Part B J Eng Manuf 2000;214:529–34. https://doi.org/10.1243/0954405001518224.

[2] Klocke F, Döbbeler B, Peng B, Lakner T. FE-simulation of the cutting process under consideration of cutting fluid. Procedia CIRP 2017;58:341–6. https://doi.org/10.1016/j.procir.2017.03.235.

[3] Helmig T, Peng B, Ehrenpreis C, Augspurger T, Frekers Y, Kneer R, et al. A coupling approach combining computational fluid dynamics and finite element method to predict cutting fluid effects on the tool temperature in cutting processes. J Manuf Sci Eng 2019;141:1–6. https://doi.org/10.1115/1.4044102.

[4] Duchosal A, Werda S, Serra R, Leroy R, Hamdi H. Numerical modeling and experimental measurement of MQL impingement over an insert in a milling tool with inner channels. Int J Mach Tool Manuf 2015;94:37–47. https://doi.org/10.1016/j.ijmachtools.2015.04.003.

[5] Veiga F, Arizmendi M, Jiménez A, Del Val AG. Analytical thermal model of orthogonal cutting process for predicting the temperature of the cutting tool with temperature-dependent thermal conductivity. Int J Mech Sci 2021;204:106524. https://doi.org/10.1016/j.ijmecsci.2021.106524.

[6] la Monaca A, Axinte DA, Liao Z, M'Saoubi R, Hardy MC. Towards understanding the thermal history of microstructural surface deformation when cutting a next generation powder metallurgy nickel-base superalloy. Int J Mach Tool Manuf 2021;168:103765. https://doi.org/10.1016/j.ijmachtools.2021.103765.

[7] Liao Z, Polyakov M, Diaz OG, Axinte D, Mohanty G, Maeder X, et al. Grain refinement mechanism of nickel-based superalloy by severe plastic deformation - mechanical machining case. Acta Mater 2019;180:2–14. https://doi.org/10.1016/j.actamat.2019.08.059.

[8] Duchosal A, Serra R, Leroy R, Louste C. Numerical steady state prediction of spitting effect for different internal canalization geometries used in MQL machining strategy. J Manuf Process 2015;20:149–61. https://doi.org/10.1016/j.jmapro.2015.08.008.

[9] Weinert K, Inasaki I, Sutherland JW, Wakabayashi T. Dry machining and minimum quantity lubrication. CIRP Ann Manuf Technol 2004;53:511–37. https://doi.org/10.1016/S0007-8506(07)60027-4.

[10] Mao C, Zhou X, Yin L, Zhang M, Tang K, Zhang J. Investigation of the flow field for a double-outlet nozzle during minimum quantity lubrication grinding. Int J Adv Manuf Technol 2016;85:291–8. https://doi.org/10.1007/s00170-015-7896-2.

[11] Axinte DA, De Chiffre L. Effectiveness and resolution of tests for evaluating the performance of cutting fluids in machining aerospace alloys. CIRP Ann Manuf Technol 2008;57:129–32. https://doi.org/10.1016/j.cirp.2008.03.081.
[12] Kamata Y, Obikawa T. High speed MQL finish-turning of Inconel 718 with different coated tools. J Mater Process Technol 2007;192–193:281–6. https://doi.org/10.1016/j.jmatprotec.2007.04.052.
[13] Ayed Y, Robert C, Germain G, Ammar A. Development of a numerical model for the understanding of the chip formation in high-pressure water-jet assisted machining. Finite Elem Anal Des 2016;108:1–8. https://doi.org/10.1016/j.finel.2015.09.003.
[14] Suárez A, López de Lacalle LN, Polvorosa R, Veiga F, Wretland A. Effects of high-pressure cooling on the wear patterns on turning inserts used on alloy IN718. Mater Manuf Process 2017;32:678–86. https://doi.org/10.1080/10426914.2016.1244838.
[15] Deshpande YV, Andhare AB, Padole PM. How cryogenic techniques help in machining of nickel alloys? A review. Mach Sci Technol 2018;22:543–84. https://doi.org/10.1080/10910344.2017.1382512.
[16] Pereira O, Celaya A, Urbikaín G, Rodríguez A, Fernández-Valdivielso A. Noberto López de lacalle L. CO2 cryogenic milling of inconel 718: cutting forces and tool wear. J Mater Res Technol 2020;9:8459–68. https://doi.org/10.1016/j.jmrt.2020.05.118.
[17] López De Lacalle LN, Angulo C, Lamikiz A, Sánchez JA. Experimental and numerical investigation of the effect of spray cutting fluids in high speed milling. J Mater Process Technol 2006;172:11–5. https://doi.org/10.1016/j.jmatprotec.2005.08.014.
[18] Mulyadi IH, Mativenga PT. Random or intuitive nozzle position in high-speed milling using minimum quantity lubricant. Proc Inst Mech Eng Part B J Eng Manuf 2014;228:21–30. https://doi.org/10.1177/0954405413495536.
[19] Vazquez E, Kemmoku DT, Noritomi PY, Da Silva JVL, Ciurana J. Computer fluid dynamics analysis for efficient cooling and lubrication conditions in micromilling of Ti6Al4V alloy. Mater Manuf Process 2014;29:1494–501. https://doi.org/10.1080/10426914.2014.941864.
[20] Robles-Linares JA, Liao Z, Axinte D, Gameros A. The effect of interstitial fluid on the machining behaviour of cortical bone. J Mater Process Technol 2022;307:117697. https://doi.org/10.1016/j.jmatprotec.2022.117697.
[21] Robles-Linares JA, Axinte D, Liao Z, Gameros A. Machining-induced thermal damage in cortical bone: necrosis and micro-mechanical integrity. Mater Des 2021;197:109215. https://doi.org/10.1016/j.matdes.2020.109215.
[22] Astakhov V. Chapter 6 Improvements of tribological conditions. In: Tribol. Met. Cut. 1st ed. Elsevier; 2006. p. 326–90. https://doi.org/10.1016/S0167-8922(06)80008-.
[23] Williams JA. The action of lubricants in metal cutting. J Mech Eng Sci 1977;19:202–12. https://doi.org/10.1243/JMES_JOUR_1977_019_044_02.
[24] Williams JA, Tabor D. The role of lubricants in machining. Wear 1977;43:275–92. https://doi.org/10.1016/0043-1648(77)90125-9.
[25] Godlevski VA, Volkov AV, Latyshev VN, Maurin LN. The kinetics of lubricant penetration action during machining. Lubr Sci 1997;9:127–40. https://doi.org/10.1002/ls.3010090203.
[26] Wilcox DC. Reassessment of the scale-determining equation for advanced turbulence models. AIAA J 1988;26:1299–310. https://doi.org/10.2514/3.10041.
[27] Pereira O, Rodríguez A, Calleja-Ochoa A, Celaya A, de Lacalle LNL, Fernández-Valdivielso A, et al. Simulation of cryo-cooling to improve super alloys cutting tools. Int J Precis Eng Manuf - Green Technol 2022;9:73–82. https://doi.org/10.1007/s40684-021-00313-y.
[28] Kawasegi N, Sugimori H, Morimoto H, Morita N, Hori I. Development of cutting tools with microscale and nanoscale textures to improve frictional behavior. Precis Eng 2009;33:248–54. https://doi.org/10.1016/j.precisioneng.2008.07.005.
[29] Koshy P, Tovey J. Performance of electrical discharge textured cutting tools. CIRP Ann Manuf Technol 2011;60:153–6. https://doi.org/10.1016/j.cirp.2011.03.104.
[30] Obikawa T, Kamio A, Takaoka H, Osada A. Micro-texture at the coated tool face for high performance cutting. Int J Mach Tool Manuf 2011;51:966–72. https://doi.org/10.1016/j.ijmachtools.2011.08.013.
[31] Li X, Liu X, Yue C, Liang SY, Wang L. Systematic review on tool breakage monitoring techniques in machining operations. Int J Mach Tool Manuf 2022;176:103882. https://doi.org/10.1016/j.ijmachtools.2022.103882.
[32] Fernández-Lucio P, Villarón-Osorno I, Pereira Neto O, Ukar E, López de Lacalle LN, Gil del Val A. Effects of laser-textured on rake face in turning PCD tools for Ti6Al4V. J Mater Res Technol 2021;15:177–88. https://doi.org/10.1016/j.jmrt.2021.08.004.
[33] Lei S, Devarajan S, Chang Z. A study of micropool lubricated cutting tool in machining of mild steel. J Mater Process Technol 2009;209:1612–20. https://doi.org/10.1016/j.jmatprotec.2008.04.024.
[34] Liao Z, Xu D, Axinte D, M'Saoubi R, Thelin J, Wretland A. Novel cutting inserts with multi-channel irrigation at the chip-tool interface: modelling, design and experiments. CIRP Ann 2020;69:65–8. https://doi.org/10.1016/j.cirp.2020.04.028.
[35] Wang B, Liu Z, Cai Y, Luo X, Ma H, Song Q, et al. Advancements in material removal mechanism and surface integrity of high speed metal cutting: a review. Int J Mach Tool Manuf 2021;166:103744. https://doi.org/10.1016/j.ijmachtools.2021.103744.
[36] Liu H, Xu X, Zhang J, Liu Z, He Y, Zhao W, et al. The state of the art for numerical simulations of the effect of the microstructure and its evolution in the metal-cutting processes. Int J Mach Tool Manuf 2022;177:103890. https://doi.org/10.1016/j.ijmachtools.2022.103890.
[37] Johnson GR, Cook WH. A constitutive model and data for metals subjected to large strains, high strain rates and high temperatures. Seventh Int Symp Ballist 1983:541–7.
[38] Johnson GR, Cook WH. Fracture characteristics of three metals subjected to various strains, strain rates, temperatures and pressures. Eng Fract Mech 1985;21:31–48. https://doi.org/10.1016/0013-7944(85)90052-9.
[39] Klocke F, Döbbeler B, Peng B, Schneider SAM. Tool-based inverse determination of material model of direct aged alloy 718 for FEM cutting simulation. Procedia CIRP 2018;77:54–7. https://doi.org/10.1016/j.procir.2018.08.211.
[40] la Monaca A, Murray JW, Liao Z, Speidel A, Robles-Linares JA, Axinte DA, et al. Surface integrity in metal machining - part II: functional performance. Int J Mach Tool Manuf 2021;164:103718. https://doi.org/10.1016/j.ijmachtools.2021.103718.
[41] Palaniappan K, Sundararaman M, Murthy H, Jeyaraam R, Rao BC. Influence of workpiece texture and strain hardening on chip formation during machining of Ti–6Al–4V alloy. Int J Mach Tool Manuf 2022;173:103849. https://doi.org/10.1016/j.ijmachtools.2021.103849.
[42] Xu D, Liao Z, Axinte D, Hardy M. A novel method to continuously map the surface integrity and cutting mechanism transition in various cutting conditions. Int J Mach Tool Manuf 2020;151:103529. https://doi.org/10.1016/j.ijmachtools.2020.103529.
[43] Liao Z, la Monaca A, Murray J, Speidel A, Ushmaev D, Clare A, et al. Surface integrity in metal machining - part I: fundamentals of surface characteristics and formation mechanisms. Int J Mach Tool Manuf 2021;162:103687. https://doi.org/10.1016/j.ijmachtools.2020.103687.
[44] Asad M. Effects of tool edge geometry on chip segmentation and exit burr: a finite element approach. Metals (Basel) 2019;9. https://doi.org/10.3390/met9111234.